How Much Localization Performance Gain Could Be Reaped by 5G mmWave MIMO Systems from Harnessing Multipath Propagation?

Bingpeng Zhou[†], Risto Wichman[‡], and Lei Zhang[⋆]
[†]School of Electronics and Communication Engineering, Sun Yat-sen University, Shenzhen 518000, China
[‡]Department of Signal Processing and Acoustics, Aalto University, Espoo 02150, Finland
[⋆]Jame Watt School of Engineering, University of Glasgow, Glasgow, G12 8QQ, UK
zhoubp3@mail.sysu.edu.cn, risto.wichman@aalto.fi, lei.zhang@glasgow.ac.uk

***Abstract*—Millimeter-wave (mmWave) massive multiple input multiple input (MIMO) has shown great potential in user equipment (UE) localization of 5G wireless communication systems. However, mmWave signals usually suffer from non-line-of-sight (NLOS) propagation, which will affect mmWave MIMO-based UE localization performance. Hence, it is non-trivial to reveal how NLOS propagation affect mmWave-based UE localization performance. In this paper, we give a unified analysis framework for UE localization performance gain from harnessing NLOS propagation. Firstly, a closed-form Cramer-Rao lower bound on mmWave MIMO-based UE localization is derived to shed lights on its performance limit. Secondly, NLOS propagation-caused localization error for conventional UE localization methods without harnessing multipath effect is analysed. Finally, the information contribution from NLOS channel is quantified, which sheds light on how to smartly harness NLOS propagation and the associated UE localization performance gain.**

***Index Terms*—Localization, 5G mmWave MIMO, Cramer-Rao lower bound, performance limits, non-line-of-sight propagation.**

I. Introduction

MASSIVE multi-input-multi-output (MIMO) mmWave-based localization has received much attention, due to the expected rising demands of localization-aware services in the future [1]– [3]. It is shown in [4] that mmWave MIMO system can provide a high-resolution positioning solution approaching subcentimeters accuracy for user equipments (UEs). A number of papers, for example [4]– [10], have investigated UE localization for mmWave MIMO systems.

In practice, mmWave signals suffer from diffuse scattering, which will affect the performance of mmWave MIMO-based UE localization. Conventional localization approaches treat non-line-of-sight (NLOS) paths as disturbance sources without any information contribution to UE localization, due to complex diffuse-scattering models. Hence, only the line-of-sight (LOS) channel is employed to extract UE location knowledge. Hence, their localization performance will be affected by the NLOS propagation. However, the localization performance gain from harnessing NLOS paths is not studied.

This work was supported by National Natural Science Foundation of China under Grant 62001526, and in part by the Natural Science Foundation of Guangdong Province under Grant 2021A1515012021.

Performance limits of mmWave MIMO-based UE localization are reported by a few research works, e.g., [4], [11]–[13]. In [4], a Cramer-Rao lower bound (CRLB) on the two-dimensional UE localization error is derived, and [12] extends this CRLB analysis to a three-dimensional regime. In [11], the localization performance using a single array is studied. In spite of their great efforts, the effect of NLOS propagation on UE localization is not investigated. Thus, a comprehensive understanding on the performance limits of mmWave MIMO-based UE localization over multipath propagation is needed.

In this paper, we aim to provide a unified analysis framework for mmWave MIMO-based UE localization performance, which is challenging due to the complex scattering model and small-scale channel fading. UE localization performance gain from harnessing NLOS propagation is quantitatively analysed, which sheds lights on the performance limits of mmWave MIMO-based UE localization over NLOS propagation. It is shown that it is possible to mitigate the NLOS effect by a carefully-designed localization algorithm.

The remainder of this paper is organized as follows. Section II presents the system model. The impact of the NLOS propagation is analysed in Section III. Simulation results are given in Section IV. Finally, Section V concludes the paper.

II. System Model

In this section, we elaborate the system setup and channel model for mmWave-based UE localization.

A. System Setup

We consider a mmWave system with J base stations (BSs), one UE and N_{C}' subcarriers. Each BS has N_{B} antennas, whereas the UE has N_{U} antennas, as shown in Fig. 1. BSs will transmit pilots for estimating UE location parameters.

We consider OFDM signaling and the length of cyclic prefix exceeds the maximum delay. We assume small-scale fading coefficients to be invariant within each time slot. Each time slot consists of a number of symbols, where the first M symbols are used to transmit pilots, and the rest are used to transmit data. In addition, N_{C}' subcarriers of each pilot are fairly allocated to those J BS's via some predefined scheduling procedure, and

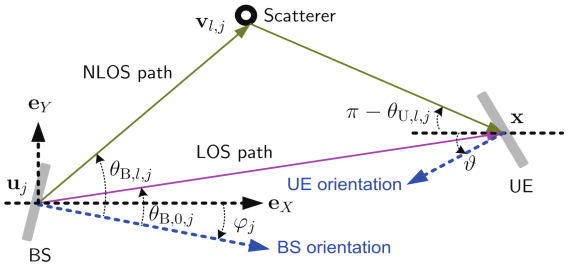

Fig. 1. Illustration of the mmWave MIMO system.

thus each BS has $N_{\mathrm{C}} = N'_{\mathrm{C}}/J$ subcarriers to transmit pilots (N_{C} is set to be an integer). Let $\boldsymbol{\omega}_j[n,m] \in \mathbb{C}^{N_{\mathrm{B}}}$ be mth pilot from N_{B} antennas of the jth BS on the nth subcarrier, which has absorbed the beamforming (BF) matrix and pilots. For brevity, let $\boldsymbol{\omega} \in \mathbb{C}^{N_{\mathrm{B}}JN_{\mathrm{C}}M} = \mathrm{vec}[\boldsymbol{\omega}_j[n,m]|\forall n = 1:N_{\mathrm{C}}, \forall m = 1:M, \forall j = 1:J]$ be the collection of pilot vectors, where $\mathrm{vec}[\cdots]$ yields a column vector by stacking all elements. In addition, let $\Theta_j = \{j, j+J, \cdots, j+(N_{\mathrm{C}}-1)J\}$ denote the index set of subcarriers of the jth BS.

B. Channel Model with Limited Scattering

We consider a limited scattering scenario in the mmWave channel. Let $\mathbf{u}_j \in \mathbb{R}^2$ and $\varphi_j \in [-\pi, \pi)$ denote the known location and angular direction of the jth BS. Let $\mathbf{x} \in \mathbb{R}^2$ and $\vartheta \in [-\pi, \pi)$ be the unknown position and orientation of the UE. There are $L+1$ paths in the scattering channel from each BS where the first path corresponds to line-of-sight (LOS) channel and the other paths are non-line-of-sight (NLOS) channels. Let $\tau_{l,j}$, $\theta_{\mathrm{B},l,j}$ and $\theta_{\mathrm{U},l,j}$ denote the time-of-arrival (TOA), angle-of-departure (AOD) and angle-of-arrival (AOA) of the lth path associated with the jth BS, respectively, which are unknown scalars. For each NLOS path, there is a scatterer with an unknown location, as shown in Fig. 1. Let $\mathbf{v}_{l,j} \in \mathbb{R}^2$ be the unknown location of the scatter associated with the lth path and the jth BS. In addition, we consider the single-bounce reflection for the NLOS paths, as per the mmWave signal propagation characteristics [4], [12].

Given the multipath parameters $\{\tau_{l,j}, \theta_{\mathrm{B},l,j}, \theta_{\mathrm{U},l,j}, \forall l\}$, the channel matrix $\widetilde{\mathbf{H}}_j[n,k] \in \mathbb{C}^{N_{\mathrm{B}} \times N_{\mathrm{U}}}$ between the jth BS and the UE on the nth subcarrier, at time slot k, is given by [4]

$$\widetilde{\mathbf{H}}_j[n,k] = \mathbf{A}_{\mathrm{U},j}[n]\mathbf{H}_j[n,k]\mathbf{A}^{\mathrm{H}}_{\mathrm{B},j}[n],$$

where $\mathbf{A}_{\mathrm{B},j}[n] \in \mathbb{C}^{N_{\mathrm{B}} \times (L+1)}$ and $\mathbf{A}_{\mathrm{U},j}[n] \in \mathbb{C}^{N_{\mathrm{U}} \times (L+1)}$ is the ULA steering matrix of the jth BS and the ULA response matrix of UE, respectively, on the nth subcarrier, given by

$$\mathbf{A}_{\mathrm{B},j}[n] = N_{\mathrm{B}}^{-\frac{1}{2}}[\mathbf{a}_{\mathrm{B},n}(\theta_{\mathrm{B},0,j}), \cdots, \mathbf{a}_{\mathrm{B},n}(\theta_{\mathrm{B},L,j})], \quad (1)$$

$$\mathbf{a}_{\mathrm{B},n}(\theta_{\mathrm{B},l,j}) = \mathrm{vec}[e^{-\mathrm{j}\frac{d_{\mathrm{B}}\pi}{\lambda_n}(t-1)\sin\theta_{\mathrm{B},l,j}}|\forall t = 1:N_{\mathrm{B}}], \quad (2)$$

$$\mathbf{A}_{\mathrm{U},j}[n] = N_{\mathrm{U}}^{-\frac{1}{2}}[\mathbf{a}_{\mathrm{U},n}(\theta_{\mathrm{U},0,j}), \cdots, \mathbf{a}_{\mathrm{U},n}(\theta_{\mathrm{U},L,j})], \quad (3)$$

$$\mathbf{a}_{\mathrm{U},n}(\theta_{\mathrm{U},l,j}) = \mathrm{vec}[e^{-\mathrm{j}\frac{d_{\mathrm{U}}\pi}{\lambda_n}(r-1)\sin\theta_{\mathrm{U},l,j}}|\forall r = 1:N_{\mathrm{U}}], \quad (4)$$

in which $\mathrm{j} = \sqrt{-1}$, $\lambda_n = \dfrac{c}{f_C + \frac{n}{T_s N'_C}}$ is the wavelength associated with subcarrier n, c denotes the speed of light, T_s is sampling period, and d_{B} is the distance between antenna elements of each BS, which are known scalers.

In addition, $\mathbf{H}_j[n,k] \in \mathbb{C}^{(L+1)\times(L+1)}$ is the frequency-domain channel matrix on the nth subcarrier:

$$\mathbf{H}_j[n,k] = \sqrt{N_{\mathrm{B}}N_{\mathrm{U}}}\mathrm{diag}\big\{h_{l,j}[k]e^{-\mathrm{j}2\pi\frac{n}{N'_{\mathrm{C}}T_s}\tau_{l,j}}|\forall l = 0:L\big\},$$

where $\mathrm{diag}[\cdots]$ yields a diagonal matrix, and $h_{l,j}[k]$ is the small-scale fading coefficient associated with the lth path, the jth BS and the kth time slot (we have absorbed path loss into small-scale fading coefficients). Let $\mathbf{h}[k] \in \mathbb{C}^{J(L+1)} = \mathrm{vec}[h_{l,j}[k]|\forall l = 0:L, \ \forall j = 1:J]$ be the collection of all small-scale fading coefficients. We assume $\mathbf{h}[k]$ follows a complex Gaussian distribution, i.e., $\mathbf{h}[k] \sim \mathcal{N}_{\mathbb{C}}(\mathbf{0}, \boldsymbol{\Sigma})$, where $\boldsymbol{\Sigma} \in \mathbb{S}^{J(L+1)}$. The relationship between $\{\mathbf{x}, \mathbf{v}_{l,j}, \vartheta\}$ and $\{\tau_{l,j}, \theta_{\mathrm{B},l,j}, \theta_{\mathrm{U},l,j}\}$ is given by

$$\tau_{0,j} = \frac{\|\mathbf{x}-\mathbf{u}_j\|_2}{c}, \quad (5)$$

$$\tau_{l,j} = \frac{\|\mathbf{x}-\mathbf{v}_{l,j}\|_2 + \|\mathbf{u}_j-\mathbf{v}_{l,j}\|_2}{c}, \ l>0, \quad (6)$$

$$\theta_{\mathrm{B},0,j} = \arccos\left(\frac{(\mathbf{x}-\mathbf{u}_j)^\top\mathbf{e}_X}{\|\mathbf{x}-\mathbf{u}_j\|_2}\right) - \varphi_j, \quad (7)$$

$$\theta_{\mathrm{B},l,j} = \arccos\left(\frac{(\mathbf{v}_{l,j}-\mathbf{u}_j)^\top\mathbf{e}_X}{\|\mathbf{v}_{l,j}-\mathbf{u}_j\|_2}\right) - \varphi_j, \ l>0, \quad (8)$$

$$\theta_{\mathrm{U},0,j} = \pi + \arccos\left(\frac{(\mathbf{x}-\mathbf{u}_j)^\top\mathbf{e}_X}{\|\mathbf{x}-\mathbf{u}_j\|_2}\right) - \vartheta, \quad (9)$$

$$\theta_{\mathrm{U},l,j} = \pi + \arccos\left(\frac{(\mathbf{x}-\mathbf{v}_{l,j})^\top\mathbf{e}_X}{\|\mathbf{x}-\mathbf{v}_{l,j}\|_2}\right) - \vartheta, \ l>0, \quad (10)$$

where $\|\bullet\|_2$ is the ℓ_2-norm on vectors, and $\mathbf{e}_X = [1,0]^T$.

C. Received Signal Model

Let $\mathbf{z}_j[n,m,k] \in \mathbb{C}^{N_{\mathrm{U}}}$ be the observation signal, i.e., the mth received pilot signal vector on subcarrier n from the jth BS at the kth time slot, which is given by [4]

$$\mathbf{z}_j[n,m,k] = \widetilde{\mathbf{H}}_j[n,k]\,\boldsymbol{\omega}_j[n,m] + \boldsymbol{\epsilon}_j[n,m,k], \quad (11)$$

where $\boldsymbol{\epsilon}_j[n,m,k] \in \mathbb{C}^{N_{\mathrm{U}}}$ is the measurement noise vector. Let $\mathbf{z}[k] \in \mathbb{C}^{N_{\mathrm{U}}N_{\mathrm{C}}MJ} = \mathrm{vec}[\mathbf{z}_j[n,m,k]|\forall n \in \Theta_j, \forall m = 1:M, \forall j = 1:J]$ and $\boldsymbol{\epsilon}[k] \in \mathbb{C}^{N_{\mathrm{U}}N_{\mathrm{C}}MJ} = \mathrm{vec}[\boldsymbol{\epsilon}_j[n,m,k]|\forall n \in \Theta_j, \forall j = 1:J, \forall m = 1:M]$ be the collection of received signals and noises, respectively. Let $\boldsymbol{\alpha} \in \mathbb{R}^3 = [\mathbf{x}^\top, \vartheta]^\top$ be UE location parameter, and let $\mathbf{v} \in \mathbb{R}^{2JL} = \mathrm{vec}[\mathbf{v}_{l,j}|\forall l = 1:L, \forall j = 1:J]$ be the collection of scatterer locations.

Then, $\mathbf{z}[k]$ is a function of $\boldsymbol{\alpha}$, $\mathbf{h}[k]$ and $\boldsymbol{\epsilon}[k]$, given by

$$\mathbf{z}[k] = \mathbf{g}(\boldsymbol{\alpha}, \mathbf{v}, \mathbf{h}[k]) + \boldsymbol{\epsilon}[k], \quad (12)$$

where we assume $\boldsymbol{\epsilon} \sim \mathcal{N}_{\mathbb{C}}(\mathbf{0}, \sigma^2\mathbf{I}_{N_{\mathrm{U}}N_{\mathrm{C}}MJ})$ with variance σ^2, $\mathbf{I}_{N_{\mathrm{U}}N_{\mathrm{C}}MJ}$ is an $N_{\mathrm{U}}N_{\mathrm{C}}MJ$-dimensional identity matrix, and $\mathbf{g}(\boldsymbol{\alpha}, \mathbf{v}, \mathbf{h}[k])$ is given by

$$\mathbf{g}(\boldsymbol{\alpha}, \mathbf{v}, \mathbf{h}[k]) = \mathbf{G}(\boldsymbol{\alpha}, \mathbf{v})\mathbf{h}[k], \quad (13)$$

in which $\mathbf{G}(\boldsymbol{\alpha}, \mathbf{v}) \in \mathbb{C}^{N_{\mathrm{U}}N_{\mathrm{C}}MJ \times J(L+1)}$ is called the coefficient matrix of channel vector $\mathbf{h}[k]$, that is dependent on the

unknown location parameter $\boldsymbol{\alpha}$ and is given by [4]

$$\mathbf{G}(\boldsymbol{\alpha},\mathbf{v}) = \mathrm{diag}[\mathbf{G}_j|\forall j=1:J], \quad (14)$$

$$\mathbf{G}_j \in \mathbb{C}^{N_\mathrm{U}N_\mathrm{C}M\times(L+1)} = \mathrm{vec}\left[\mathrm{g}_j^{(r)\mathrm{H}}[n,m]|\forall r,\forall n,\forall m\right], \quad (15)$$

$$\mathbf{g}_j^{(r)}[n,m] \in \mathbb{C}^{L+1} = \mathrm{vec}[\mathrm{g}_{l,j}^{(r)}[n,m]|\forall l=0:L], \quad (16)$$

$$\mathrm{g}_{l,j}^{(r)}[n,m] = \sqrt{N_\mathrm{B}N_\mathrm{U}}\boldsymbol{\omega}_j^\top[n,m]\boldsymbol{\mu}_{l,j,n}^{(r)}, \quad (17)$$

$$\boldsymbol{\mu}_{l,j,n}^{(r)} \in \mathbb{C}^{N_\mathrm{B}} = \mathrm{vec}[\mu_{l,j,n}^{(r,t)}|\forall t=1:N_\mathrm{B}], \quad (18)$$

$$\mu_{l,j,n}^{(r,t)} = \mathrm{a}_{\mathrm{U},n}^{(r)}(\theta_{\mathrm{U},l,j})e^{-\mathrm{j}2\pi\frac{n}{N_\mathrm{C}'T_s}\tau_{l,j}}(\mathrm{a}_{\mathrm{B},n}^{(t)}(\theta_{\mathrm{B},l,j}))^*, \quad (19)$$

where $\mathrm{a}_{\mathrm{U},n}^{(r)}(\theta_{\mathrm{U},l,j})$ and $\mathrm{a}_{\mathrm{B},n}^{(t)}(\theta_{\mathrm{B},l,j})$ is the rth and the tth element of $\mathbf{a}_{\mathrm{U},n}(\theta_{\mathrm{U},l,j})$ and $\mathbf{a}_{\mathrm{B},n}(\theta_{\mathrm{B},l,j})$ in (4) and (2), respectively. It should be noted that $\mathrm{a}_{\mathrm{U},n}^{(r)}(\theta_{\mathrm{U},l,j})$ and $\mathrm{a}_{\mathrm{B},n}^{(t)}(\theta_{\mathrm{B},l,j})$ are functions of location parameters $\mathbf{x}$, ϑ and $\mathbf{v}_{l,j}$ via (5)–(10).

III. The Effect Of NLOS Propagation

In this section, we analyse UE localization performance to understand the effect of NLOS propagation on UE localization.

A. UE Localization Method

We consider two UE localization methods, and both extract UE location knowledge from the LOS path only. The difference between these two methods lies in the treatment of NLOS paths: in the first-type LOS channel-based localization method, the NLOS paths are viewed as the disturbance source; while in the second-type LOS channel-based localization method, the NLOS channel state is treated as unknown parameters to be jointly estimated along with UE localization.

For convenience, let $\mathbf{h}_{\mathsf{LOS}}[k] = \mathrm{vec}[h_{0,j}[k]|\forall j=1:J] \in \mathbb{C}^J$ and $\mathbf{h}_{\mathsf{NLOS}}[k] = \mathrm{vec}[h_{l,j}[k]|\forall l=1:L,\ \forall j=1:J] \in \mathbb{C}^{JL}$ denote the small-scale fading coefficient vector associated with the LOS channel and the NLOS channel, respectively.

1) First-Type LOS Channel-Based Localization Approach: This UE localization estimates $\boldsymbol{\alpha}$ via exploiting LOS propagation knowledge, where those unknown NLOS paths are treated as disturbance sources without any information contribution. It is formulated as

$$\mathscr{P}_{\mathrm{LOS}}^{(\mathsf{I})}: \hat{\boldsymbol{\alpha}}_{\mathsf{LOS}}^{(\mathsf{I})} = \arg\min_{\boldsymbol{\alpha}} \mathbb{E}_{\mathbf{h}_{\mathsf{LOS}}[k]}\left\{\|\mathbf{z}[k]-\mathbf{g}_{\mathsf{LOS}}(\boldsymbol{\alpha},\mathbf{h}_{\mathsf{LOS}}[k])\|_2^2\right\} \quad (20)$$

where $\mathbf{g}_{\mathsf{LOS}}(\boldsymbol{\alpha},\mathbf{h}_{\mathsf{LOS}}[k]) \in \mathbb{C}^{N_\mathrm{U}N_\mathrm{C}MJ}$ is the LOS component of the measurement signal, given by

$$\mathbf{g}_{\mathsf{LOS}}(\boldsymbol{\alpha},\mathbf{h}_{\mathsf{LOS}}[k]) = \mathbf{G}_{\mathsf{LOS}}(\boldsymbol{\alpha})\mathbf{h}_{\mathsf{LOS}}[k], \quad (21)$$

and $\mathbf{G}_{\mathsf{LOS}}(\boldsymbol{\alpha}) \in \mathbb{C}^{N_\mathrm{U}N_\mathrm{C}MJ\times J}$ is the coefficient matrix of LOS channel coefficient vector $\mathbf{h}_{\mathsf{LOS}}[k]$, given by

$$\mathbf{G}_{\mathsf{LOS}}(\boldsymbol{\alpha}) = \mathrm{diag}\{\boldsymbol{g}_{0,j}|\forall j=1:J\}, \quad (22)$$

$$\boldsymbol{g}_{0,j} \in \mathbb{C}^{N_\mathrm{U}N_\mathrm{C}M} = \mathrm{vec}[(\mathrm{g}_{0,j}^{(r)}[n,m])^*|\forall r,\forall n,\forall m], \quad (23)$$

where $\mathrm{g}_{0,j}^{(r)}[n,m]$ is given by (17). Given $\hat{\boldsymbol{\alpha}}_{\mathsf{LOS}}^{(\mathsf{I})}$, LOS channel estimate $\hat{\mathbf{h}}_{\mathsf{LOS}}^{(\mathsf{I})}[k]$ can be obtained using the linear least square estimate, as per the linear model (21).

$\mathscr{P}_{\mathrm{LOS}}^{(\mathsf{I})}$ is non-convex w.r.t. the UE location parameter due to the nonlinear cost function in $\boldsymbol{\alpha}$. This LOS channel-based localization covers a number of conventional UE localization methods, for instance, TOA-based localization [14] and trilateration-based localization method.

2) Second-Type LOS Channel-Based Localization Method: This method jointly estimates UE location parameters (using the LOS path) and NLOS channel states which absorb small-scale fading coefficients, BS steering gain, UE response gain and time-delay-caused phase shift.

Let $\mathrm{c}_{l,j,n}^{(r,t)}[k] = \mathrm{a}_{\mathrm{U},n}^{(r)}(\theta_{\mathrm{U},l,j})h_{l,j}[k]\mu_{l,j,n}^{(r,t)}\mathrm{a}_{\mathrm{B},n}^{(t)*}(\theta_{\mathrm{B},l,j})$ denote the overall NLOS channel state associated with the (r,t)th receiver-transmitter antenna pair of the jth BS at the nth subcarrier and the kth time slot, for the lth NLOS path. For convenience, we use the following notations,

$$\mathbf{c}_{j,n}^{(r,t)}[k] = \mathsf{vec}[\mathrm{c}_{l,j,n}^{(r,t)}[k]|\forall l=1:L] \in \mathbb{C}^L, \quad (24)$$

$$\mathbf{h}_{\mathsf{NLOS}}^{\mathsf{EQ}}[k] = \mathsf{vec}[\mathbf{c}_{j,n}^{(r,t)}[k]|\forall t,\forall r,\forall n,\forall m,\forall j], \quad (25)$$

where $\mathbf{h}_{\mathsf{NLOS}}^{\mathsf{EQ}}[k] \in \mathbb{C}^{LJMN_\mathrm{U}N_\mathrm{C}N_\mathrm{B}}$ denotes the NLOS channel vector. Let $\mathbf{h}_{\mathsf{EQ}}[k] \in \mathbb{C}^{J+LJMN_\mathrm{U}N_\mathrm{C}N_\mathrm{B}} = [\mathbf{h}_{\mathsf{LOS}}[k];\mathbf{h}_{\mathsf{NLOS}}^{\mathsf{EQ}}[k]]$ be the equivalent channel. Let $\boldsymbol{\chi}[k] \in \mathbb{C}^{3+J+LJMN_\mathrm{U}N_\mathrm{C}N_\mathrm{B}} = [\boldsymbol{\alpha};\mathbf{h}_{\mathsf{EQ}}[k]]$ be the overall variable. Specifically, the second-type LOS channel-based localization method is formulated as

$$\mathscr{P}_{\mathrm{LOS}}^{(\mathsf{II})}: \hat{\boldsymbol{\chi}}_{\mathsf{LOS}}^{(\mathsf{II})} = \arg\min_{\boldsymbol{\chi}[k]} \|\mathbf{z}[k]-\mathbf{g}_{\mathsf{EQ}}(\boldsymbol{\chi}[k])\|_2^2, \quad (26)$$

where the measurement function $\mathbf{g}_{\mathsf{EQ}}(\boldsymbol{\chi}[k])$ is reformulated as

$$\mathbf{g}_{\mathsf{EQ}}(\boldsymbol{\chi}[k]) = \underbrace{\mathbf{g}_{\mathsf{LOS}}(\boldsymbol{\alpha},\mathbf{h}_{\mathsf{LOS}}[k])}_{\text{LOS path}} + \underbrace{\mathbf{W}^{\mathsf{H}}\mathbf{h}_{\mathsf{NLOS}}^{\mathsf{EQ}}[k]}_{\text{NLOS path}}, \quad (27)$$

where $\mathbf{g}_{\mathsf{LOS}}(\boldsymbol{\alpha},\mathbf{h}_{\mathsf{LOS}}[k])$ relates to the LOS path, given by (21), and $\mathbf{W} \in \mathbb{C}^{LJMN_\mathrm{U}N_\mathrm{C}N_\mathrm{B}\times JMN_\mathrm{U}N_\mathrm{C}}$ denotes the known pilot symbol matrix, given by

$$\mathbf{W} = \mathsf{diag}[\mathbf{W}_j[n,m]|\forall n,\forall m,\forall j], \quad (28)$$

$$\mathbf{W}_j[n,m] \in \mathbb{C}^{N_\mathrm{U}N_\mathrm{B}L\times N_\mathrm{U}} = \mathbf{I}_{N_\mathrm{U}} \otimes \mathbf{w}_j[n,m], \quad (29)$$

$$\mathbf{w}_j[n,m,k] \in \mathbb{C}^{N_\mathrm{B}L} = \mathbf{1}_L \otimes \boldsymbol{\omega}_j[n,m], \quad (30)$$

in which $\mathbf{1}_L$ is an L-dimensional all-one vector.

B. UE Localization Performance

We shall explicate the closed-form CRLB for the above two typical LOS channel-based localization methods to reveal the UE location information from the LOS channel.

1) First-Type LOS Channel-Based Localization Error: For $\mathscr{P}_{\mathrm{LOS}}^{(\mathsf{I})}$, since NLOS paths are treated as disturbances, there are two error sources, i.e., unknown NLOS signals and measurement noise. The unknown NLOS signal will lead to a fixed localization error for a certain measurement signal, since the small-scale fading coefficients of NLOS paths are assumed to be invariant within a time slot and the UE location is fixed. Hence, the NLOS paths will lead to a certain localization bias, instead of a "random localization error". In contrast, measurement noises will lead to a random localization error, which can be bounded by its CRLB.

We give a theorem to bound the error of the first-type LOS channel-based UE localization problem $\mathscr{P}_{\mathrm{LOS}}^{(\mathsf{I})}$.

Theorem 1 (First-Type LOS Channel-Based UE Localization Error): The mean squared error of the first-type LOS channel-based localization problem is bounded as follows,

$$\mathbb{E}\{\|\hat{\boldsymbol{\alpha}}_{\mathsf{LOS}}^{(\mathrm{I})}-\boldsymbol{\alpha}\|_2^2\}\geq \mathsf{trace}\big(\underbrace{\boldsymbol{\mathcal{B}}_{\boldsymbol{\alpha}}^{(\mathrm{I})}(\boldsymbol{\alpha})+\boldsymbol{\Omega}_{\boldsymbol{\alpha}}}_{\boldsymbol{\mathcal{Q}}_{\boldsymbol{\alpha}}^{(\mathrm{I})}(\boldsymbol{\alpha})}\big), \tag{31}$$

where $\hat{\boldsymbol{\alpha}}_{\mathsf{LOS}}^{(\mathrm{I})}$ is the UE location estimate as per $\mathscr{P}_{\mathrm{LOS}}^{(\mathrm{I})}$, $\boldsymbol{\Omega}_{\boldsymbol{\alpha}}\in\mathbb{S}^3=\big(\mathbb{E}\{\hat{\boldsymbol{\alpha}}_{\mathsf{LOS}}^{(\mathrm{I})}\}-\boldsymbol{\alpha}\big)\big(\mathbb{E}\{\hat{\boldsymbol{\alpha}}_{\mathsf{LOS}}^{(\mathrm{I})}\}-\boldsymbol{\alpha}\big)^{\top}$ is the NLOS paths-caused UE localization bias, and $\boldsymbol{\mathcal{B}}_{\boldsymbol{\alpha}}^{(\mathrm{I})}(\boldsymbol{\alpha})$ is the CRLB on the unbiased UE location error, given by

$$\boldsymbol{\mathcal{B}}_{\boldsymbol{\alpha}}^{(\mathrm{I})}(\boldsymbol{\alpha})=\Big(\underbrace{\sigma^{-2}\mathbf{D}_{\mathsf{LOS}}\boldsymbol{\mathcal{H}}_{\mathsf{LOS}}[k]\boldsymbol{\Psi}_{\mathsf{LOS}}\boldsymbol{\mathcal{H}}_{\mathsf{LOS}}^{\mathrm{H}}[k]\mathbf{D}_{\mathsf{LOS}}^{\mathrm{H}}}_{\boldsymbol{\mathcal{J}}_{\boldsymbol{\alpha}}^{(\mathrm{I})}(\boldsymbol{\alpha})}\Big)^{-1}, \tag{32}$$

where $\mathbf{D}_{\mathsf{LOS}}\in\mathbb{C}^{3\times JMN_{\mathrm{C}}N_{\mathrm{U}}}$ is given by (45), and $\boldsymbol{\mathcal{H}}_{\mathsf{LOS}}[k]\in\mathbb{C}^{JMN_{\mathrm{C}}N_{\mathrm{U}}\times JMN_{\mathrm{C}}N_{\mathrm{U}}}$ is given by

$$\boldsymbol{\mathcal{H}}_{\mathsf{LOS}}[k]=\mathsf{diag}\{\boldsymbol{\mathcal{H}}_j^{\mathsf{LOS}}[k]|\forall j=1:J\}, \tag{33}$$

in which $\boldsymbol{\mathcal{H}}_j^{\mathsf{LOS}}[k]\in\mathbb{C}^{MN_{\mathrm{C}}N_{\mathrm{U}}\times MN_{\mathrm{C}}N_{\mathrm{U}}}$ is given by

$$\boldsymbol{\mathcal{H}}_j^{\mathsf{LOS}}[k]=\mathbf{I}_{MN_{\mathrm{C}}N_{\mathrm{U}}}\otimes h_{0,j}^{*}[k], \tag{34}$$

and $\boldsymbol{\Psi}_{\mathsf{LOS}}\in\mathbb{S}^{JMN_{\mathrm{C}}N_{\mathrm{U}}}$ is given by

$$\boldsymbol{\Psi}_{\mathsf{LOS}}=\mathbf{I}_{JMN_{\mathrm{C}}N_{\mathrm{U}}}-\mathbf{G}_{\mathsf{LOS}}(\mathbf{G}_{\mathsf{LOS}}^{\mathrm{H}}\mathbf{G}_{\mathsf{LOS}})^{-1}\mathbf{G}_{\mathsf{LOS}}^{\mathrm{H}}, \tag{35}$$

where $\mathbf{G}_{\mathsf{LOS}}\in\mathbb{C}^{JN_{\mathrm{C}}N_{\mathrm{U}}M\times J}$ is given by (22).

Proof: See the proof in APPENDIX A. □

The first-type LOS channel-based location Fisher information matrix (FIM) $\boldsymbol{\mathcal{J}}_{\boldsymbol{\alpha}}^{(\mathrm{I})}(\boldsymbol{\alpha})$ in (32) quantifies the UE location information from the LOS channel. It is difficult to establish the closed-form expression of UE location estimate bias $\boldsymbol{\Omega}_{\boldsymbol{\alpha}}$ due to complex system models. However, the above closed-form CRLB is still meaningful for bounding the achieved UE localization error of $\mathscr{P}_{\mathrm{LOS}}^{(\mathrm{I})}$. To address this challenge, in the following, we aim to approximately characterize the NLOS-path-caused UE location estimate bias.

For ease of notation, let $\varepsilon_{\boldsymbol{\alpha}}=(\mathsf{trace}(\boldsymbol{\Omega}_{\boldsymbol{\alpha}}))^{\frac{1}{2}}$ be the location bias in meters, and let $\mathbf{g}_{\mathsf{NLOS}}[k]\in\mathbb{C}^{JMN_{\mathrm{U}}N_{\mathrm{C}}}=\mathbf{W}^{\mathsf{H}}\mathbf{h}_{\mathsf{NLOS}}^{\mathsf{EQ}}[k]$ be the NLOS path of the first-type LOS channel-based localization method, as shown in (27).

Theorem 2 (NLOS-Caused Localization Bias): The NLOS path-caused UE location estimate bias $\varepsilon_{\boldsymbol{\alpha}}$ in the first-type LOS channel-based localization method is given by

$$\varepsilon_{\boldsymbol{\alpha}}=\|\mathbf{g}_{\mathsf{NLOS}}[k]\|_2\|\mathbf{D}_{\mathsf{LOS}}[k]\boldsymbol{\mathcal{H}}_{\mathsf{LOS}}[k]\|_2^{-1}+o_{\boldsymbol{\alpha}}, \tag{36}$$

where $o_{\boldsymbol{\alpha}}$ is a second-order infinitesimal which can be safely ignored, i.e., $o_{\boldsymbol{\alpha}}\sim\mathcal{O}\big(\|\hat{\boldsymbol{\alpha}}_{\mathsf{LOS}}^{(\mathrm{I})}-\boldsymbol{\alpha}\|_2^2+\|\hat{\mathbf{h}}_{\mathsf{LOS}}^{(\mathrm{I})}[k]-\mathbf{h}_{\mathsf{LOS}}[k]\|_2^2\big)$.

Proof: See APPENDIX B. □

Remark 1 (NLOS Path-Caused Location Error Floor): It is shown in Theorem 1 that the UE location error bound $\boldsymbol{\mathcal{B}}_{\boldsymbol{\alpha}}^{(\mathrm{I})}(\boldsymbol{\alpha})$ of the first-type LOS channel-based localization method is proportional to the measurement noise variance σ^2. In addition, the NLOS-path-caused UE location bias $\varepsilon_{\boldsymbol{\alpha}}$ is invariant with σ^2. Hence, as the SNR increases, the first-type LOS channel-based localization error will gradually reduce and finally hit an error floor $\varepsilon_{\boldsymbol{\alpha}}$ due to NLOS propagation. Hence, in the high SNR region, the unknown NLOS path will become the dominant error source, which limits the performance of the first-type LOS channel-based localization method. □

Corollary 1 (Scaling of LOS Channel-Based Localization Bias): The first-type LOS channel-based UE localization error scales with the NLOS signal strength in the following manner:

$$\lim_{\|\mathbf{g}_{\mathsf{NLOS}}[k]\|_2\to 0}\frac{\varepsilon_{\boldsymbol{\alpha}}}{\|\mathbf{g}_{\mathsf{NLOS}}[k]\|_2}=\|\mathbf{D}_{\mathsf{LOS}}\boldsymbol{\mathcal{H}}_{\mathsf{LOS}}[k]\|_2^{-1}, \tag{37}$$

where $\|\bullet\|_2$ denotes the ℓ_2-norm on a matrix.

Proof 1: It directly follows from Theorem 2.

Remark 2: It is shown that the NLOS-caused UE location error floor vanishes as the NLOS signal strength tends to zero. In addition, this location error floor is affected by the LOS channel quantity, i.e., the LOS channel gain $\mathbf{h}_{\mathsf{LOS}}[k]$. □

The above conclusions are applied to conventional TOA-based localization methods in which it is well known that NLOS paths will lead to a localization bias.

2) Second-Type LOS Channel-Based Localization CRLB: We give a theorem to establish the closed-form CRLB for the second-type LOS channel-based localization method.

Theorem 3 (Second-Type LOS Channel-Based UE Location CRLB): For an unbiased UE location estimate $\hat{\boldsymbol{\alpha}}_{\mathsf{LOS}}^{(\mathrm{II})}$ of the second-type LOS Channel-based localization problem $\mathscr{P}_{\mathrm{LOS}}^{(\mathrm{II})}$, its mean squared error is bounded as

$$\mathbb{E}\{\|\hat{\boldsymbol{\alpha}}_{\mathsf{LOS}}^{(\mathrm{II})}-\boldsymbol{\alpha}\|_2^2\}\geq\mathsf{trace}\big(\boldsymbol{\mathcal{B}}_{\boldsymbol{\alpha}}^{(\mathrm{II})}(\boldsymbol{\chi}[k])\big), \tag{38}$$

where $\boldsymbol{\mathcal{B}}_{\boldsymbol{\alpha}}^{(\mathrm{II})}(\boldsymbol{\chi}[k])$ is the associated CRLB given by

$$\boldsymbol{\mathcal{B}}_{\boldsymbol{\alpha}}^{(\mathrm{II})}(\boldsymbol{\chi}[k])=\Big(\underbrace{\sigma^{-2}\mathbf{D}_{\mathsf{LOS}}\boldsymbol{\mathcal{H}}_{\mathsf{LOS}}[k]\boldsymbol{\Lambda}\boldsymbol{\mathcal{H}}_{\mathsf{LOS}}^{\mathrm{H}}[k]\mathbf{D}_{\mathsf{LOS}}^{\mathrm{H}}}_{\boldsymbol{\mathcal{J}}_{\boldsymbol{\alpha}}^{(\mathrm{II})}(\boldsymbol{\chi}[k])}\Big)^{-1}, \tag{39}$$

where $\mathbf{D}_{\mathsf{LOS}}$ is given by (45), $\boldsymbol{\Lambda}\in\mathbb{C}^{JMN_CN_U}=\mathbf{I}_{JMN_CN_U}-\boldsymbol{\mathcal{W}}^{\mathrm{H}}\big(\boldsymbol{\mathcal{W}}\boldsymbol{\mathcal{W}}^{\mathrm{H}}\big)^{-1}\boldsymbol{\mathcal{W}}$, and $\boldsymbol{\mathcal{W}}\in\mathbb{C}^{(LJMN_{\mathrm{U}}N_{\mathrm{C}}N_{\mathrm{B}}+J)\times JMN_{\mathrm{U}}N_{\mathrm{C}}}$ is given by

$$\boldsymbol{\mathcal{W}}=[\mathbf{G}_{\mathsf{LOS}}^{\mathrm{H}},\mathbf{W}]. \tag{40}$$

Proof: See the proof in APPENDIX C. □

Remark 3: The associated FIM $\boldsymbol{\mathcal{J}}_{\boldsymbol{\alpha}}^{(\mathrm{II})}(\boldsymbol{\chi}[k])$ quantifies the UE location information from the LOS channel and the estimate of NLOS channel states, which essentially depends on BS locations, SNR, channel gain, base station BF directions, and the size of BS/UE antenna arrays. Specifically, the second-type LOS channel-based UE localization CRLB $\mathsf{trace}\big(\boldsymbol{\mathcal{B}}_{\boldsymbol{\alpha}}^{(\mathrm{II})}(\boldsymbol{\chi}[k])\big)$ is proportional to the noise variance σ^2 and hence the inverse of the SNR. This means that the NLOS propagation-caused UE localization error floor in the high SNR region is vanished in the second-type LOS channel-based localization method due to the joint estimate of NLOS channel coefficients, which is different from the first-type LOS channel-based localization method. The second-type LOS channel-based localization provides a promising solution to mmWave MIMO-based UE localization. □

C. Gain from Exploiting NLOS Paths

It should be noted that, in those two LOS channel-based localization methods $\mathscr{P}_{\text{LOS}}^{(\text{I})}$ and $\mathscr{P}_{\text{LOS}}^{(\text{II})}$, UE location information is extracted from the LOS channel only. Yet, unlike $\mathscr{P}_{\text{LOS}}^{(\text{I})}$, the second-type localization method $\mathscr{P}_{\text{LOS}}^{(\text{II})}$ does not have NLOS-caused localization error floor $\varepsilon_{\boldsymbol{\alpha}}^2$ due to the joint estimate of NLOS channel state $\mathbf{h}_{\text{NLOS}}^{\text{EQ}}[k]$. The performance gain of the second-type LOS channel-based localization from NLOS channel estimate is revealed below.

Remark 4 (Performance Gain of LOS Channel-Based Localization from NLOS Channel Estimate): Compared with $\mathscr{P}_{\text{LOS}}^{(\text{I})}$, the performance gain of the second-type localization method $\mathscr{P}_{\text{LOS}}^{(\text{II})}$ from NLOS channel estimate is given by $\boldsymbol{\mathcal{Q}}_{\boldsymbol{\alpha}}^{(\text{I})} - \boldsymbol{\mathcal{B}}_{\boldsymbol{\alpha}}^{(\text{II})} = \sigma^2 \Big(\mathbf{D}_{\text{LOS}} \boldsymbol{\mathcal{H}}_{\text{LOS}}[k] \big(\boldsymbol{\Psi}_{\text{LOS}}^{-1} - \boldsymbol{\Lambda}^{-1} \big)^{-1} \boldsymbol{\mathcal{H}}_{\text{LOS}}^{\text{H}}[k] \mathbf{D}_{\text{LOS}}^{\text{H}} \Big)^{-1} + \boldsymbol{\Omega}_{\boldsymbol{\alpha}}$. □

This can be easily verified by combining (32) and (39).

IV. Numerical Results

We shall give numerical results to verify the performance limits of various localization methods.

A. Simulation Settings

We set the number of base stations to $J = 3$ and each BS has $N_{\text{C}} = 10$ subcarriers. We set $L = 2$, $M = 10$, $N_{\text{B}} = N_{\text{U}} = 16$, carrier frequency $f_{\text{C}} = 60\,\text{GHz}$, sampling period $T_s = 10\,\text{ns}$ (i.e., the bandwidth is 100 MHz) and the speed of light $c = 3 * 10^8\,\text{m/s}$. We set SNR = 10dB, unless specified otherwise, where $\text{SNR} = \dfrac{\mathbb{E}\{\|\mathbf{g}_{\text{EQ}}(\boldsymbol{\chi}[k])\|_2^2\}}{\mathbb{E}\{\|\boldsymbol{\epsilon}[k]\|_2^2\}}$. Based on these parameters, λ_n and d_{A} can be determined via $\lambda_n = \frac{c}{\frac{n}{N_{\text{C}}' T_s} + f_{\text{C}}}$ and $d_{\text{A}} = c/f_{\text{C}}/2$, respectively. We assume a simple path loss model for each channel, i.e., $h_{l,j} = \frac{h'_{l,j}}{\lambda_{l,j}^3}$, where $\lambda_{l,j}$ is the length of the path and $h'_{l,j} \sim \mathcal{N}_{\mathbb{C}}(0,1)$ is the small-scale fading. Locations of UE and BSs are random within a squared area of $50 \times 50\,\text{m}^2$, and their orientation angles are also random. In addition, the transmitted pilot signal $\boldsymbol{\omega}_j[n,m]$ is set to be uniformly distributed on the unit circle, unless specified otherwise.

B. Simulation Results

1) The Impact of NLOS Propagation: The UE localization error v.s. the number of NLOS paths is shown in Fig. 2 and Fig. 3. It is shown that more NLOS paths lead to a larger error for the first-type LOS channel-based localization method. In contrast, for the second-type LOS channel-based localization method, its performance is almost not affected by the number of NLOS paths. This means that this localization method can achieve a reliable solution in scattering environments, due to the joint estimate of NLOS channel state.

2) The Effect of SNR: UE location and orientation error performance v.s. SNR are presented in Fig. 4 and 5, respectively. It is shown that the first-type LOS channel-based localization method will hit an error floor due to the NLOS propagation as the SNR increases. This is because the NLOS propagation will become the dominant error source for this localization method when SNR $> 10\,\text{dB}$. Moreover, the second-type LOS channel-based localization error decreases to zero as the SNR increases. In other words, this method breaks the NLOS propagation-caused error floor in the high SNR region due to the exploitation of NLOS channels.

V. Conclusions

In this paper, the UE localization performance limits over multipath propagation and small-scale fading are studied for 5G mmWave MIMO systems. The closed-form CRLBs for the UE localization and the channel estimate, respectively, are obtained. The UE localization performance gain from harnessing NLOS propagation is revealed. It is shown that the UE localization error will be significantly reduced by carefully designing a NLOS propagation harnessing scheme, particularly in a high SNR environments.

Appendix A
Proof of Theorem 1

Based on the estimation theory [15], the mean squared error of the first-type LOS channel-based UE location estimate $\hat{\boldsymbol{\alpha}}_{\text{LOS}}^{(\text{I})}$ follows (41), where $\mathbf{cov}(\hat{\boldsymbol{\alpha}}_{\text{LOS}}^{(\text{I})})$ denotes the covariance matrix

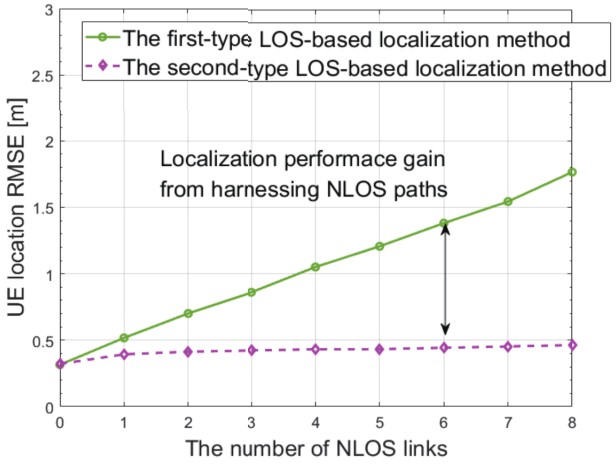

Fig. 2. UE location error bounds v.s. the number of NLOS links.

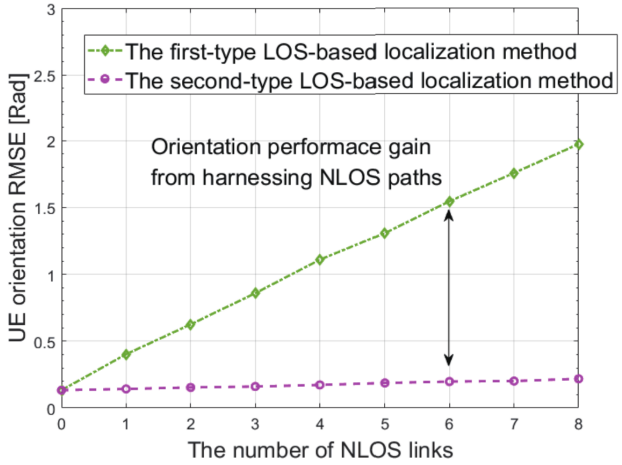

Fig. 3. UE orientation error bounds v.s. the number of NLOS links.

$$\mathbb{E}\{(\hat{\boldsymbol{\alpha}}_{\mathsf{LOS}}^{(\mathrm{I})}-\boldsymbol{\alpha})(\hat{\boldsymbol{\alpha}}_{\mathsf{LOS}}^{(\mathrm{I})}-\boldsymbol{\alpha})^{\top}\}=\boldsymbol{\Omega}_{\boldsymbol{\alpha}}+\underbrace{\mathbb{E}\{(\hat{\boldsymbol{\alpha}}_{\mathsf{LOS}}^{(\mathrm{I})}-\mathbb{E}\{\hat{\boldsymbol{\alpha}}_{\mathsf{LOS}}^{(\mathrm{I})}\})(\hat{\boldsymbol{\alpha}}_{\mathsf{LOS}}^{(\mathrm{I})}-\mathbb{E}\{\hat{\boldsymbol{\alpha}}_{\mathsf{LOS}}^{(\mathrm{I})}\})^{\top}\}}_{\mathbf{cov}(\hat{\boldsymbol{\alpha}}_{\mathsf{LOS}}^{(\mathrm{I})})}. \tag{41}$$

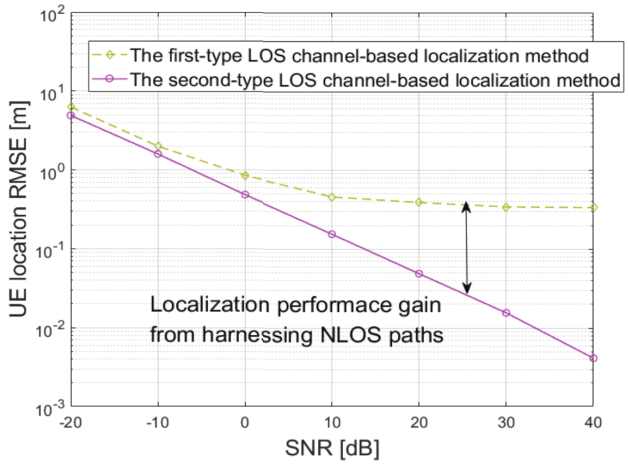

Fig. 4. UE location CRLB of various localization methods v.s. SNR.

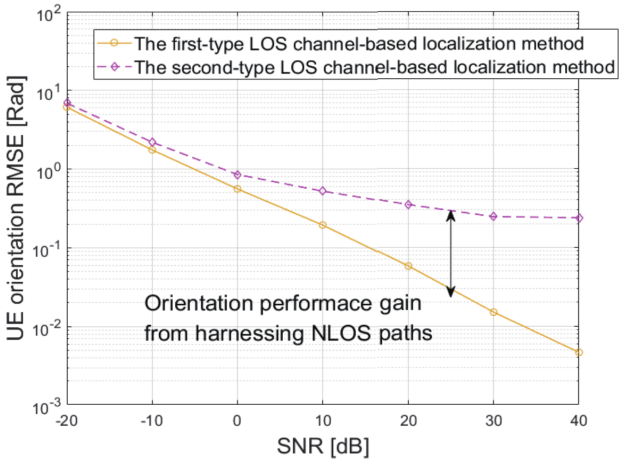

Fig. 5. UE orientation CRLB of various localization methods v.s. SNR.

of UE location estimate errors, which is bounded by its CRLB $\boldsymbol{\mathcal{B}}_{\boldsymbol{\alpha}}^{(\mathrm{I})}(\boldsymbol{\alpha})$, i.e., $\mathbf{cov}(\hat{\boldsymbol{\alpha}}_{\mathsf{LOS}}^{(\mathrm{I})}) \succeq \boldsymbol{\mathcal{B}}_{\boldsymbol{\alpha}}^{(\mathrm{I})}(\boldsymbol{\alpha})$.

Let $\boldsymbol{\beta}_{\mathsf{LOS}}[k] \in \mathbb{C}^{3+JL} = [\boldsymbol{\alpha}; \mathbf{h}_{\mathsf{LOS}}[k]]$ be the LOS component of the first-type LOS channel-based UE localization method $\mathscr{P}_{\mathrm{LOS}}^{(\mathrm{I})}$. Let $\boldsymbol{\mathcal{B}}_{\boldsymbol{\beta}_{\mathsf{LOS}}[k]}^{(\mathrm{I})}(\boldsymbol{\beta}_{\mathsf{LOS}}[k]) \in \mathbb{S}^{3+JL}$ be the associated CRLB. The estimate error of $\boldsymbol{\beta}_{\mathsf{LOS}}[k]$ will be bounded by its CRLB $\boldsymbol{\mathcal{B}}_{\boldsymbol{\beta}_{\mathsf{LOS}}[k]}(\boldsymbol{\beta}_{\mathsf{LOS}}[k])$ which is given by

$$\boldsymbol{\mathcal{B}}_{\boldsymbol{\beta}_{\mathsf{LOS}}[k]}(\boldsymbol{\beta}_{\mathsf{LOS}}[k]) = \big(\boldsymbol{\mathcal{J}}_{\boldsymbol{\beta}_{\mathsf{LOS}}[k]}(\boldsymbol{\beta}_{\mathsf{LOS}}[k])\big)^{-1}, \tag{42}$$

where $\boldsymbol{\mathcal{J}}_{\boldsymbol{\beta}_{\mathsf{LOS}}[k]}(\boldsymbol{\beta}_{\mathsf{LOS}}[k])$ is the FIM of $\boldsymbol{\beta}_{\mathsf{LOS}}[k]$, given by

$$\boldsymbol{\mathcal{J}}_{\boldsymbol{\beta}_{\mathsf{LOS}}[k]}(\boldsymbol{\beta}_{\mathsf{LOS}}[k]) = \mathbb{E}\{\nabla^2_{\boldsymbol{\beta}_{\mathsf{LOS}}[k]} \ln p(\boldsymbol{\beta}_{\mathsf{LOS}}[k]|\mathbf{z}[k])\}, \tag{43}$$

where $\nabla^2_{\boldsymbol{\beta}_{\mathsf{LOS}}[k]}$ is the second-order derivative w.r.t. $\boldsymbol{\beta}_{\mathsf{LOS}}[k]$ and $p(\mathbf{z}[k]|\boldsymbol{\beta}_{\mathsf{LOS}}[k])$ is the likelihood function.

Based on the system model (20) and (21), the $\boldsymbol{\beta}_{\mathsf{LOS}}[k]$'s FIM, i.e., $\boldsymbol{\mathcal{J}}_{\boldsymbol{\beta}_{\mathsf{LOS}}[k]}^{(\mathrm{I})}(\boldsymbol{\beta}_{\mathsf{LOS}}[k])$, is finally given by (44), where $\boldsymbol{\mathcal{H}}_{\mathsf{LOS}}[k]$ is given by (33) and $\mathbf{G}_{\mathsf{LOS}} \in \mathbb{C}^{JN_{\mathrm{C}}N_{\mathrm{U}}M\times J}$ is given by (21), and $\mathbf{D}_{\mathsf{LOS}} \in \mathbb{C}^{3\times JMN_{\mathrm{C}}N_{\mathrm{U}}}$ is given by

$$\mathbf{D}_{\mathsf{LOS}} = [\mathbf{d}_{j,m,n}^{\mathsf{LOS}(r)} | \forall r, \forall n, \forall m, \forall j], \tag{45}$$

$$\mathbf{d}_{j,m,n}^{\mathsf{LOS}(r)} \in \mathbb{C}^3 = \begin{bmatrix} \sum\limits_{t=1:N_{\mathrm{B}}} \omega_j^{(t)}[m,n]\mu_{0,j,n}^{(r,t)*}\boldsymbol{\varrho}_{0,j,n}^{(r,t)} \\ \sum\limits_{t=1:N_{\mathrm{B}}} \omega_j^{(t)}[m,n]\mu_{0,j,n}^{(r,t)*}\rho_{0,j,n}^{(r,t)} \end{bmatrix}, \tag{46}$$

wherein $\boldsymbol{\varrho}_{0,j,n}^{(r,t)}$ is given by (47) and $\rho_{0,j,n}^{(r,t)}$ is given by (48).

Based on the above FIM structure and as per the Schur complement, the UE location CRLB is given by

$$\boldsymbol{\mathcal{B}}_{\boldsymbol{\alpha}}^{(\mathrm{I})}(\boldsymbol{\alpha}) = \sigma^2\big(\mathbf{D}_{\mathsf{LOS}}\boldsymbol{\mathcal{H}}_{\mathsf{LOS}}[k]\boldsymbol{\Psi}_{\mathsf{LOS}}\boldsymbol{\mathcal{H}}_{\mathsf{LOS}}^{\mathrm{H}}[k]\mathbf{D}_{\mathsf{LOS}}^{\mathrm{H}}\big)^{-1}, \tag{49}$$

where $\boldsymbol{\Psi}_{\mathsf{LOS}}$ and $\boldsymbol{\mathcal{H}}_{\mathsf{LOS}}[k]$ is given by (35) and (33), respectively. Combining (49) and (41), Theorem 1 is proved.

Appendix B
Proof of Theorem 2

Let $\boldsymbol{\alpha}_{\mathsf{true}}$ and $\mathbf{h}_{\mathsf{LOS}}^{\mathsf{true}}[k]$ be the true value of $\boldsymbol{\alpha}$ and $\mathbf{h}_{\mathsf{LOS}}[k]$, respectively. As per (12), we have $\mathbf{z}[k] = \mathbf{g}_{\mathsf{LOS}}(\boldsymbol{\alpha}, \mathbf{h}_{\mathsf{LOS}}[k]) + \mathbf{g}_{\mathsf{NLOS}} + \boldsymbol{\epsilon}[k]$, where $\mathbf{g}_{\mathsf{NLOS}}[k]$ stands for the unknown NLOS component and $\mathbf{g}_{\mathsf{LOS}}(\boldsymbol{\alpha}, \mathbf{h}_{\mathsf{LOS}}[k]) = \mathbf{G}_{\mathsf{LOS}}(\boldsymbol{\alpha})\mathbf{h}_{\mathsf{LOS}}[k]$. Let $(\hat{\boldsymbol{\alpha}}_{\mathsf{LOS}}^{(\mathrm{I})}, \hat{\mathbf{h}}_{\mathsf{LOS}}^{(\mathrm{I})}[k])$ be the biased estimate from $\mathbf{z}[k]$. Then, we have $\mathbf{G}_{\mathsf{LOS}}(\hat{\boldsymbol{\alpha}}_{\mathsf{LOS}}^{(\mathrm{I})})\hat{\mathbf{h}}_{\mathsf{LOS}}^{(\mathrm{I})}[k] = \mathbf{g}_{\mathsf{LOS}} + \mathbf{g}_{\mathsf{NLOS}} + \boldsymbol{\epsilon}[k]$.

By applying the first-order expansion to $\mathbf{G}_{\mathsf{LOS}}(\hat{\boldsymbol{\alpha}})\hat{\mathbf{h}}_{\mathsf{LOS}}[k]$ around $(\boldsymbol{\alpha}, \mathbf{h}_{\mathsf{LOS}}[k]) = (\boldsymbol{\alpha}_{\mathsf{true}}, \mathbf{h}_{\mathsf{LOS}}^{\mathsf{true}}[k])$, we have

$$\begin{aligned}\mathbf{G}_{\mathsf{LOS}}(\hat{\boldsymbol{\alpha}}_{\mathsf{LOS}}^{(\mathrm{I})})\hat{\mathbf{h}}_{\mathsf{LOS}}^{(\mathrm{I})}[k] &= \underbrace{\mathbf{G}_{\mathsf{LOS}}(\boldsymbol{\alpha}_{\mathsf{true}})\mathbf{h}_{\mathsf{LOS}}^{\mathsf{true}}[k]}_{\mathbf{g}_{\mathsf{LOS}}} \\ &+ \begin{bmatrix} \nabla_{\boldsymbol{\alpha}}\big(\mathbf{G}_{\mathsf{LOS}}(\boldsymbol{\alpha}_{\mathsf{true}})\mathbf{h}_{\mathsf{LOS}}^{\mathsf{true}}[k]\big) \\ \big(\mathbf{G}_{\mathsf{LOS}}(\boldsymbol{\alpha}_{\mathsf{true}})\big)^{\top} \end{bmatrix}^{\top} \begin{bmatrix} \hat{\boldsymbol{\alpha}}_{\mathsf{LOS}}^{(\mathrm{I})} - \boldsymbol{\alpha}_{\mathsf{true}} \\ \hat{\mathbf{h}}_{\mathsf{LOS}}^{(\mathrm{I})}[k] - \mathbf{h}_{\mathsf{LOS}}^{\mathsf{true}}[k] \end{bmatrix} \\ &+ \mathcal{O}(\|\hat{\boldsymbol{\alpha}}_{\mathsf{LOS}}^{(\mathrm{I})} - \boldsymbol{\alpha}_{\mathsf{true}}\|_2^2 + \|\hat{\mathbf{h}}_{\mathsf{LOS}}^{(\mathrm{I})}[k] - \mathbf{h}_{\mathsf{LOS}}^{\mathsf{true}}[k]\|_2^2). \end{aligned} \tag{50}$$

Hence, by ignoring the high-order infinitesimal term and taking the expectation over $\boldsymbol{\epsilon}$, we have $\begin{bmatrix} \nabla_{\boldsymbol{\alpha}}\big(\mathbf{G}_{\mathsf{LOS}}(\boldsymbol{\alpha}_{\mathsf{true}})\mathbf{h}_{\mathsf{LOS}}^{\mathsf{true}}[k]\big) \\ \big(\mathbf{G}_{\mathsf{LOS}}(\boldsymbol{\alpha}_{\mathsf{true}})\big)^{\top} \end{bmatrix}^{\top} \begin{bmatrix} \mathbb{E}\{\hat{\boldsymbol{\alpha}}_{\mathsf{LOS}}^{(\mathrm{I})}\} - \boldsymbol{\alpha}_{\mathsf{true}} \\ \mathbb{E}\{\hat{\mathbf{h}}_{\mathsf{LOS}}^{(\mathrm{I})}[k]\} - \mathbf{h}_{\mathsf{LOS}}^{\mathsf{true}}[k] \end{bmatrix} \approx \mathbf{g}_{\mathsf{NLOS}}$, where we have considered that $\mathbb{E}\{\boldsymbol{\epsilon}\} = \mathbf{0}$. As a result, we arrive at (51). We know that $\nabla_{\boldsymbol{\alpha}}\big(\mathbf{G}_{\mathsf{LOS}}(\boldsymbol{\alpha}_{\mathsf{true}})\mathbf{h}_{\mathsf{LOS}}^{\mathsf{true}}[k]\big) = \mathbf{D}_{\mathsf{LOS}}\boldsymbol{\mathcal{H}}_{\mathsf{LOS}}[k]$ and $\varepsilon_{\boldsymbol{\alpha}} = \|\mathbb{E}\{\hat{\boldsymbol{\alpha}}_{\mathsf{LOS}}^{(\mathrm{I})}\} - \boldsymbol{\alpha}_{\mathsf{true}}\|_2$. Hence, taking the trace of the 3×3 left-top submatrix and the 3×3 right-bottom submatrix of the correlation matrix $\mathbf{g}_{\mathsf{NLOS}}\mathbf{g}_{\mathsf{NLOS}}^{\top}$ in (51), respectively, and using the singular-value-decomposition of the left coefficient matrix, Theorem 2 is proved.

Appendix C
Proof of Theorem 3

Based on the second-type LOS channel-based localization model in (26) and (27) and as per the FIM definition in (43),

$$\boldsymbol{\mathcal{J}}^{(\mathsf{I})}_{\boldsymbol{\beta}_{\mathsf{LOS}}[k]}(\boldsymbol{\beta}_{\mathsf{LOS}}[k]) = \sigma^{-2}\begin{bmatrix} \mathbf{D}_{\mathsf{LOS}}\boldsymbol{\mathcal{H}}_{\mathsf{LOS}}[k]\boldsymbol{\mathcal{H}}^{\mathrm{H}}_{\mathsf{LOS}}[k]\mathbf{D}^{\mathrm{H}}_{\mathsf{LOS}} & \mathbf{D}_{\mathsf{LOS}}\boldsymbol{\mathcal{H}}_{\mathsf{LOS}}[k]\mathbf{G}_{\mathsf{LOS}} \\ \mathbf{G}^{\mathrm{H}}_{\mathsf{LOS}}\boldsymbol{\mathcal{H}}^{\mathrm{H}}_{\mathsf{LOS}}[k]\mathbf{D}^{\mathrm{H}}_{\mathsf{LOS}} & \mathbf{G}^{\mathrm{H}}_{\mathsf{LOS}}\mathbf{G}_{\mathsf{LOS}} \end{bmatrix}. \tag{44}$$

$$\begin{aligned}\boldsymbol{\varrho}^{(r,t)}_{l,j,n} =& \mathrm{j}2\pi\frac{n}{cN'_{\mathrm{C}}T_s}\frac{\mathbf{x}-\mathbf{u}_j}{\|\mathbf{x}-\mathbf{u}_j\|_2} - \mathrm{j}\frac{d_{\mathrm{B}}\pi}{\lambda_n}(t-1)\frac{\|\mathbf{x}-\mathbf{u}_j\|_2^2\mathbf{e}_Y - (\mathbf{x}-\mathbf{u}_j)(\mathbf{x}-\mathbf{u}_j)^{\mathrm{H}}\mathbf{e}_Y}{\|\mathbf{x}-\mathbf{u}_j\|_2^3} \\ &+ \mathrm{j}\frac{d_{\mathrm{U}}\pi}{\lambda_n}(r-1)\frac{\cos\left(\arccos\left(\frac{(\mathbf{x}-\mathbf{u}_j)^\top\mathbf{e}_X}{\|\mathbf{x}-\mathbf{u}_j\|_2}\right)-\vartheta\right)}{\sqrt{1-\left(\frac{(\mathbf{x}-\mathbf{u}_j)^\top\mathbf{e}_X}{\|\mathbf{x}-\mathbf{u}_j\|_2}\right)^2}}\frac{\|\mathbf{x}-\mathbf{u}_j\|_2^2\,\mathbf{e}_X - (\mathbf{x}-\mathbf{u}_j)(\mathbf{x}-\mathbf{u}_j)^{\mathrm{H}}\mathbf{e}_X}{\|\mathbf{x}-\mathbf{u}_j\|_2^3}.\end{aligned} \tag{47}$$

$$\rho^{(r,t)}_{l,j,n} = \mathrm{j}\frac{d_{\mathrm{U}}\pi}{\lambda_n}(r-1)\cos\left(\arccos\left(\frac{(\mathbf{x}-\mathbf{u}_j)^\top\mathbf{e}_X}{\|\mathbf{x}-\mathbf{u}_j\|_2}\right)-\vartheta\right)\Bigg). \tag{48}$$

$$\mathbf{g}_{\mathsf{NLOS}}\mathbf{g}^\top_{\mathsf{NLOS}} \approx \begin{bmatrix}\nabla^\top_{\boldsymbol{\alpha}}\big(\mathbf{G}_{\mathsf{LOS}}(\boldsymbol{\alpha}_{\mathsf{true}})\mathbf{h}^{\mathsf{true}}_{\mathsf{LOS}}[k]\big)\\ \mathbf{G}^\top_{\mathsf{LOS}}(\boldsymbol{\alpha}_{\mathsf{true}})\end{bmatrix}\begin{bmatrix}\mathbb{E}\{\hat{\boldsymbol{\alpha}}^{(\mathsf{I})}_{\mathsf{LOS}}\}-\boldsymbol{\alpha}_{\mathsf{true}}\\ \mathbb{E}\{\hat{\mathbf{h}}^{(\mathsf{I})}_{\mathsf{LOS}}[k]\}-\mathbf{h}^{\mathsf{true}}_{\mathsf{LOS}}[k]\end{bmatrix}\begin{bmatrix}\mathbb{E}\{\hat{\boldsymbol{\alpha}}^{(\mathsf{I})}_{\mathsf{LOS}}\}-\boldsymbol{\alpha}_{\mathsf{true}}\\ \mathbb{E}\{\hat{\mathbf{h}}^{(\mathsf{I})}_{\mathsf{LOS}}[k]\}-\mathbf{h}^{\mathsf{true}}_{\mathsf{LOS}}[k]\end{bmatrix}^\top\begin{bmatrix}\nabla_{\boldsymbol{\alpha}}\big(\mathbf{G}_{\mathsf{LOS}}(\boldsymbol{\alpha}_{\mathsf{true}})\mathbf{h}^{\mathsf{true}}_{\mathsf{LOS}}[k]\big)\\ \mathbf{G}^\top_{\mathsf{LOS}}(\boldsymbol{\alpha}_{\mathsf{true}})\end{bmatrix} \tag{51}$$

$$\boldsymbol{\mathcal{B}}^{(\mathsf{II})}_{\boldsymbol{\alpha}}(\boldsymbol{\chi}[k]) = \sigma^2\Big(\mathbf{D}_{\mathsf{LOS}}\boldsymbol{\mathcal{H}}_{\mathsf{LOS}}[k]\boldsymbol{\mathcal{H}}^{\mathrm{H}}_{\mathsf{LOS}}[k]\mathbf{D}^{\mathrm{H}}_{\mathsf{LOS}} - \mathbf{D}_{\mathsf{LOS}}\boldsymbol{\mathcal{H}}_{\mathsf{LOS}}[k]\boldsymbol{\mathcal{W}}^{\mathrm{H}}\big(\boldsymbol{\mathcal{W}}\boldsymbol{\mathcal{W}}^{\mathrm{H}}\big)^{-1}\boldsymbol{\mathcal{W}}\boldsymbol{\mathcal{H}}^{\mathrm{H}}_{\mathsf{LOS}}[k]\mathbf{D}^{\mathrm{H}}_{\mathsf{LOS}}\Big)^{-1}, \tag{52}$$

$$= \sigma^2\mathbf{D}_{\mathsf{LOS}}\boldsymbol{\mathcal{H}}_{\mathsf{LOS}}[k]\Big(\mathbf{I}_{JMN_CN_U} - \boldsymbol{\mathcal{W}}^{\mathrm{H}}\big(\boldsymbol{\mathcal{W}}\boldsymbol{\mathcal{W}}^{\mathrm{H}}\big)^{-1}\boldsymbol{\mathcal{W}}\Big)\boldsymbol{\mathcal{H}}^{\mathrm{H}}_{\mathsf{LOS}}[k]\mathbf{D}^{\mathrm{H}}_{\mathsf{LOS}} \tag{53}$$

$$= \sigma^2\mathbf{D}_{\mathsf{LOS}}\boldsymbol{\mathcal{H}}_{\mathsf{LOS}}[k]\boldsymbol{\Lambda}\boldsymbol{\mathcal{H}}^{\mathrm{H}}_{\mathsf{LOS}}[k]\mathbf{D}^{\mathrm{H}}_{\mathsf{LOS}} \tag{54}$$

given $\mathbf{z}[k]$, the CRLB of $\boldsymbol{\chi}[k]$ is finally given by (see the derivation flow in APPENDIX A),

$$\boldsymbol{\mathcal{B}}^{(\mathsf{II})}_{\boldsymbol{\chi}[k]}(\boldsymbol{\chi}[k]) = \sigma^2\begin{bmatrix}\boldsymbol{\Theta}_{\mathsf{LOS}} & \mathbf{D}_{\mathsf{LOS}}\boldsymbol{\mathcal{H}}_{\mathsf{LOS}}[k]\boldsymbol{\mathcal{W}}^{\mathrm{H}}\\ \boldsymbol{\mathcal{W}}\boldsymbol{\mathcal{H}}^{\mathrm{H}}_{\mathsf{LOS}}[k]\mathbf{D}^{\mathrm{H}}_{\mathsf{LOS}} & \boldsymbol{\mathcal{W}}\boldsymbol{\mathcal{W}}^{\mathrm{H}}\end{bmatrix}^{-1},$$

with $\boldsymbol{\Theta}_{\mathsf{LOS}} = \mathbf{D}_{\mathsf{LOS}}\boldsymbol{\mathcal{H}}_{\mathsf{LOS}}[k]\boldsymbol{\mathcal{H}}^{\mathrm{H}}_{\mathsf{LOS}}[k]\mathbf{D}^{\mathrm{H}}_{\mathsf{LOS}}$, where $\boldsymbol{\mathcal{H}}_{\mathsf{LOS}}[k]$ and $\mathbf{D}_{\mathsf{LOS}}$ is given by (33) and (45), respectively. Then, as per the Schur complement, the UE location CRLB $\boldsymbol{\mathcal{B}}^{(\mathsf{II})}_{\boldsymbol{\alpha}}(\boldsymbol{\chi}[k])$ follows (52)–(54), where $\boldsymbol{\Lambda} \in \mathbb{C}^{JMN_CN_U} = \mathbf{I}_{JMN_CN_U} - \boldsymbol{\mathcal{W}}^{\mathrm{H}}\big(\boldsymbol{\mathcal{W}}\boldsymbol{\mathcal{W}}^{\mathrm{H}}\big)^{-1}\boldsymbol{\mathcal{W}}$. Hence, Theorem 3 is proved.

REFERENCES

[1] R. D. Taranto, S. Muppirisetty, R. Raulefs, D. Slock, T. Svensson, and H. Wymeersch, "Location-aware communications for 5G networks: How location information can improve scalability, latency, and robustness of 5G." *IEEE Signal Processing Magazine* 31.6 (2014): 102-112.

[2] K. Witrisal, P. Meissner, E. Leitinger, Y. Shen, C. Gustafson, F. Tufvesson, K. Haneda, D. Dardari, A. F. Molisch, A. Conti, M. Z. Win, "High-accuracy localization for assisted living: 5G systems will turn multipath channels from foe to friend." *IEEE Signal Processing Magazine* 33.2 (2016): 59-70.

[3] J. A. del Peral-Rosado, J. A Lopez-Salcedo, S. Kim, and G. Seco-Granados, "Feasibility study of 5G-based localization for assisted driving." *Localization and GNSS (ICL-GNSS), 2016 International Conference on*. IEEE, 2016.

[4] A. Shahmansoori, G. E. Garcia, G. Destino, G. Seco-Granados, and H. Wymeersch, "Position and Orientation Estimation through Millimeter Wave MIMO in 5G Systems," *IEEE Transactions on Wireless Communications*, 17.3 (2017): 1822-1835

[5] B. Zhou, A. Liu, and V. Lau. "Successive Localization and Beamforming in 5G mmWave MIMO Communication Systems." *IEEE Transactions on Signal Processing*, 67.6 (2019): 1620-1635.

[6] Z. Abu-Shaban, H. Wymeersch, T. Abhayapala, and G. Seco-Granados, "Distributed Two-Way Localization Bounds for 5G mmWave Systems." *2018 IEEE Globecom Workshops (GC Wkshps)*. IEEE, 2018.

[7] H. Wymeersch, G. Seco-Granados, G. Destino, D. Dardari, and F. Tufvesson, "5G mmWave positioning for vehicular networks." *IEEE Wireless Communications*, 24.6 (2017): 80-86.

[8] J. Palacios, G. Bielsa, P. Casari, and J. Widmer, "Single-and Multiple-Access Point Indoor Localization for Millimeter-Wave Networks." *IEEE Transactions on Wireless Communications*, 18.3 (2019): 1927-1942.

[9] J. Palacios, P. Casari, and J. Widmer. "JADE: Zero-knowledge device localization and environment mapping for millimeter wave systems." *IEEE INFOCOM 2017-IEEE Conference on Computer Communications*. IEEE, 2017.

[10] A. Guerra, F. Guidi, and D. Dardari. "On the impact of beamforming strategy on mm-wave localization performance limits." *Communications Workshops, 2017 IEEE International Conference on*. IEEE, 2017.

[11] A. Guerra, F. Guidi, and D. Dardari. "Single-Anchor Localization and Orientation Performance Limits Using Massive Arrays: MIMO v.s. Beamforming." *IEEE Transactions on Wireless Communications*, 17.8, (2018): 5241-5255.

[12] Z. Abu-Shaban, X. Zhou, T. Abhayapala, and G. Seco-Granados, "Error Bounds for Uplink and Downlink 3D Localization in 5G mmWave Systems," *IEEE Transactions on Wireless Communications*, 17.8 (2018): 4939-4954.

[13] R. Mendrzik, H. Wymeersch, G. Bauch, and Z. Abu-Shaban, "Harnessing NLOS Components for Position and Orientation Estimation in 5G Millimeter Wave MIMO," *IEEE Transactions on Wireless Communications*, vol. 18, no. 1, pp. 93-107, Jan. 2019

[14] I. Guvenc, and C.-C. Chong. "A survey on TOA based wireless localization and NLOS mitigation techniques." *IEEE Communications Surveys & Tutorials*, 11.3 (2009): 107-124.

[15] S. M. Kay, "Fundamentals of Statistical Signal Processing, Vol. 1: Estimation Theory" Prentice Hall PTR, 1998.